Ecological Engineering 37 (2011) 1174–1183

Contents lists available at ScienceDirect

Ecological Engineering

journal homepage: www.elsevier.com/locate/ecoleng

Development of a salinity-secondary flow-approach model to predict mangrove spreading

Shang-Shu Shih[a,b,*], Sheng-Chi Yang[c], Hong-Yuan Lee[a,c], Gwo-Wen Hwang[a,c], Yu-Min Hsu[c]

[a] Hydrotech Research Institute, National Taiwan University, Taipei, Taiwan
[b] Department of Landscape Architecture and Environmental Planning, University of California at Berkeley, CA, USA
[c] Department of Civil Engineering, National Taiwan University, Taipei, Taiwan

ARTICLE INFO

Article history:
Received 1 September 2010
Received in revised form 17 February 2011
Accepted 19 February 2011
Available online 27 March 2011

Keywords:
Mangrove
Water salinity
Secondary flow
Reach-scale
Sea level rise

ABSTRACT

This paper presents a new salinity-secondary flow-approach (SSA) model for identifying areas likely to be colonized by mangrove species based on two indices: water salinity concentration and river secondary flow intensity, R/W (the ratio of radius of curvature to river width). The mangrove *Kandelia obovata* is spreading rapidly in the Tanshui River system and therefore resulting in flooding impact to riparian wetlands; however, few studies have examined the dispersal characteristics of this species on the reach scale. According to the literature review and our observation, the salinity is the major factor in determining the spreading capabilities of mangroves. In addition, the effect of secondary flow can also facilitate mangrove invasion through the creation of bare mudflats.

The case study of the Tanshui River system shows that the SSA model can be used for the determination of the habitat requirements and thus the dispersal capabilities of *K. obovata*. The results of the study show that the optimum conditions for the growth and dispersal of *K. obovata* exist in waters with mean annual salinity levels that are higher than 5 ppt (parts per thousand). Although *K. obovata* can survive in brackish wetlands with mean annual salinity levels lower than 5 ppt, its spreading capability is impaired. In tidal freshwater wetlands with mean annual salinity levels that are lower than 0.1 ppt, *K. obovata* cannot survive. The study also found that the R/W lower than 3 led to large mudflats, which provide an ideal environment for the growth of mangroves, due to the secondary flow.

It shows that the SSA model can identify the potential habitat of mangrove in tidal region, so it might help with not only estuarine wetland management but also mangrove restoration project, especially for the sea level rise effect and its impact on potential mangrove invasion.

1. Introduction

Because the mangrove ecosystem can offer broad biological, economic, scientific, environmental, aesthetic, and social values (Mitsch and Gosselink, 1993; Blasco et al., 1996; Mitsch, 2005), there have been many restoration and reforestation projects worldwide. Unfortunately, most of these projects have failed completely or failed to achieve the stated goals due to neglect of the relationship between hydrology and the mangrove ecosystem (Lewis, 2000, 2005). For example, in China, after a 10-year mangrove restoration project, the mangrove area increased to 22,000 ha, but over 80% of these mangroves have been degraded due to secondary succession. One kind of mangrove (*Sonneratia apetala Buch.Ham*) occupied about 95% of the restoration areas (Ren et al., 2009). Another case is a 511 km^2 mangrove forest reserve that was killed in Colombia after road and dike construction altered hydrology conditions (Perdomo et al., 1998).

However, mangroves in Taiwan tell a different story. They distributed across the western coast (Hsueh and Lee, 2000), and the total area of mangrove forests has increased from approximately 287 ha in 1994 to 320 ha in 2006 (Fan, 2006). The mangrove forests along the Tanshui River system have grown so dense in the downstream region that it now causes flooding and biodiversity problems (Lee and Chu, 1999; Lee and Shih, 2004; Huang et al., 2010). An uncontrolled dispersal of mangroves might exclude other species due to the harsh microenvironment that they inhabit, which is characterized by high salinity, long hydroperiods and anaerobic soil conditions (Lugo, 1998). Mangroves in the Guandu wetland, where there is one of major mangrove wetlands along the Tanshui River system, have expanded to twice the original area during the last two decades (Lee and Yeh, 2009), causing the

* Corresponding author at: Hydrotech Research Institute, National Taiwan University, Taipei city 106, Taiwan. Tel.: +886 2 23687833; fax: +886 2 23687913.
E-mail address: uptreeshih@ntu.edu.tw (S.-S. Shih).

0925-8574/$ – see front matter © 2011 Elsevier B.V. All rights reserved.
doi:10.1016/j.ecoleng.2011.02.018

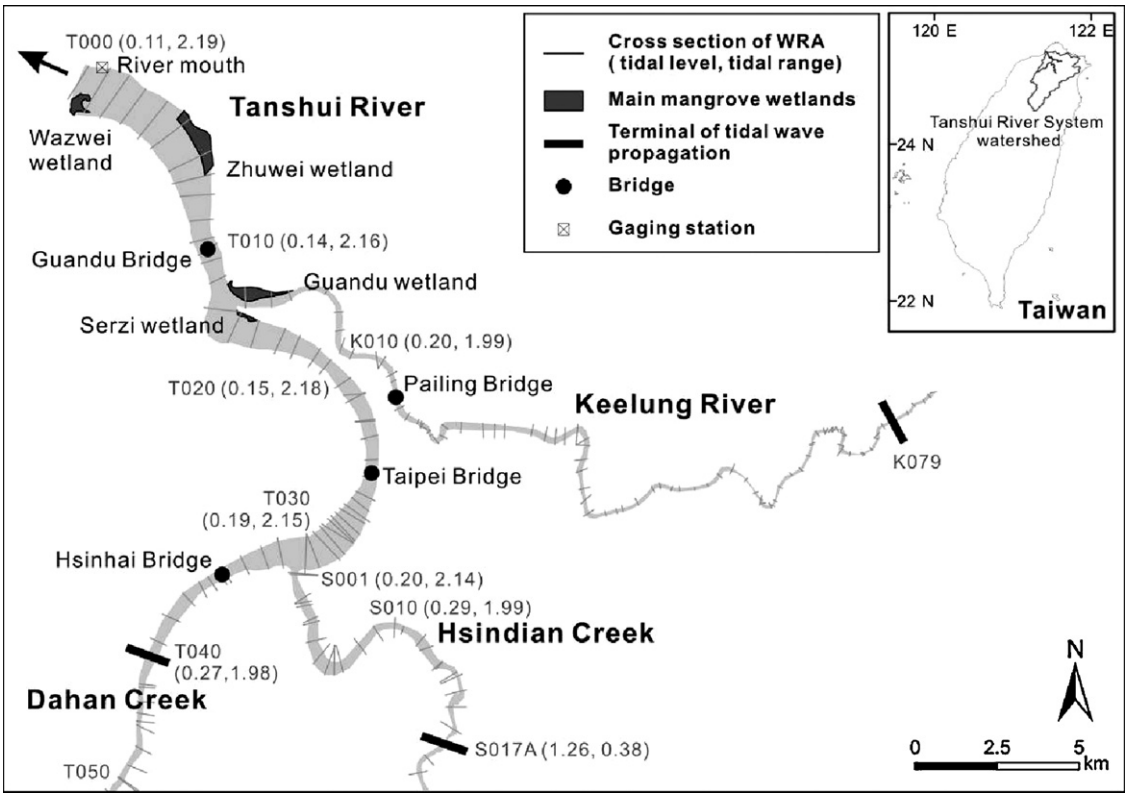

Fig. 1. Map of the study area: the tidal reach of the Tanshui River system. T000 is the first cross-section of the Tanshui River and the Dahan Creek; K001 is the first cross-section of the Keelung River; S001 is the first cross-section of the Hsindian Creek. The distance from river mouth to junctions at the Keelung River and at the Hsindian River is 8.6 km and 21.1 km, respectively. The cross-section bathymetry is from the Water Resources Agency and was the basis for subsequent analysis of mudflat length in this study.

extinction of the sedge, *Cyperus malaccensis Lam* (Wester and Lee, 1992; Lee et al., 2002), and worsening the impact of the flooding of the Keelung River (Shih, unpublished data). Recent studies have shown that these problems could become even more pronounced, as there is still the potential for mangroves to expand their range even further (Lee et al., 2002; Shih, unpublished data).

There has been much research on distribution and dispersal mechanism of mangroves on the habitat scale (e.g., Clarke and Hannon, 1967; Brown and Lugo, 1994; Lewis, 2000, 2005; Duke et al., 2002), but few studies have concentrated on large scales, e.g. reach scale, which is needed to clarify the hydrodynamic mechanism and reduce uncertainties before wetland restoration or management (Mitsch and Day, 2006). Hupp and Osterkamp (1996) indicated that riparian vegetation patterns are mainly affected by ambient hydrogeomorphic conditions and specific landforms. In addition, Lugo (1998) documents that mangrove habitats can be delimited by salinity in tidal regimes. Based on these two hypotheses, this study develops a salinity-secondary flow-approach (SSA) model to identify spreading boundaries and possible habitat of mangroves on the reach scale. The SSA model was examined by the case study of Tanshui River system, northern Taiwan. Both field survey and model simulation were investigated.

2. Materials and methods

2.1. Study area

The study area is concerned with the tidal region of the Tanshui River system, because mangroves primarily inhabit the estuarine regions. The Tanshui River system consists of three main tributaries: the Dahan Creek, the Hsindian Creek and the Keelung River. The mainstream is approximately 158 km long with a watershed covering 2726 km^2. Liu et al. (2007) indicated that the M_2 tide is the primary tidal constituent, with a mean tidal range of 2.17 m, and up to 3 m at spring tides. According to the distribution of salt concentration profile, the estuary was characterized as a homogeneous type, because difference of mean salinity concentration between top and bottom layer was less than 15%. In this study, the boundaries of the tidal region, at which the elevation of the river bed approaches the mean annual water level, were derived from Shih and Yu (2008) and are illustrated in Fig. 1.

The mangrove forests along the Tanshui River system are some of the most important mangrove habitats in Taiwan and are composed of the newly recognized species *Kandelia obovata* (Sheue et al., 2003). These habitats comprise the largest population of *K. obovata* in the northern hemisphere (Hsu, 2002) and represent the species' northernmost geographical position (Lee and Yeh, 2009). *K. obovata* has expanded with a pure forest type in the downstream region, but with a mixed one of *K. obovata* and reeds (*Phragmites communis*) in the upper regions. There are four major mangrove areas along the Tanshui River system: the Waziwei wetland, the Zhuwei wetland, the Guandu wetland, and the Shezi wetland (Fig. 1). To date, *K. obovata* is still gradually spreading along rivers in the Tanshui River system.

2.2. Salinity-secondary flow-approach (SSA) model

The SSA model is presented as a mechanistic model, and it focuses on real cause–effect relationships. This type of model is not designed primarily for predicted precision, but for the theoretical correctness of predicted responses (Guisan and Zimmermann, 2000). The SSA model predicts and identifies possible future mangrove areas by two indices: water salinity and river secondary flow intensity. The analysis process of the SSA model is consistent with

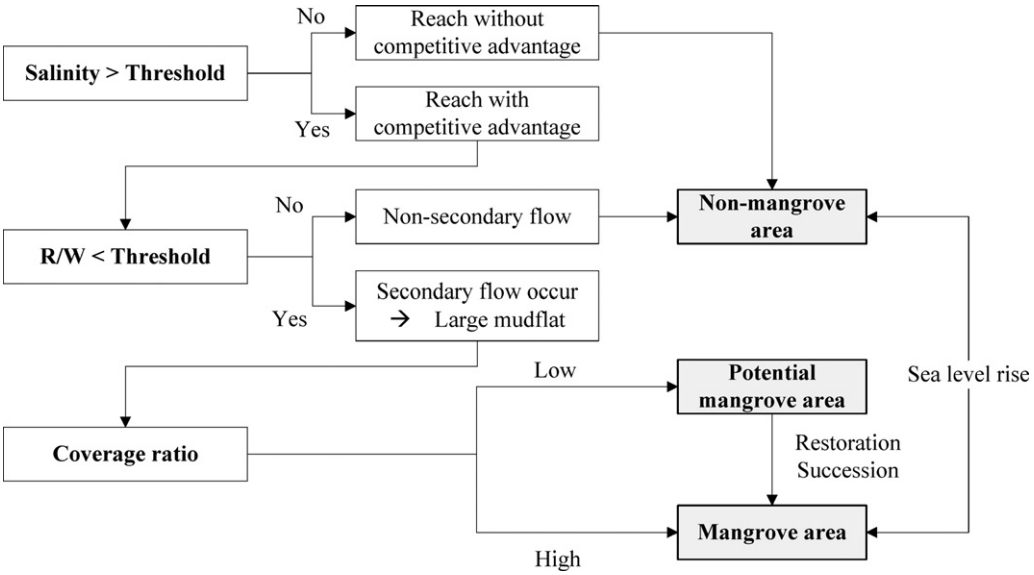

Fig. 2. The flow chart of the SSA model for identifying mangrove areas, potential mangrove areas and non-mangrove areas. First, the salinity threshold is used to determine the boundaries at which mangroves show a competitive growth advantage. The *R*/*W* threshold is then used to locate large mudflats for mangrove growth. If the coverage ratio is high in the mudflat, there is a mangrove area. In contrast, this mudflat might be limited by other factors and so should be classified as a potential mangrove area. Moreover, an area without a competitive advantage for mangroves might later become an area with a competitive advantage due to a salinity intrusion after sea levels rise effect.

three major steps and shown in Fig. 2. First, the water salinity concentration is used to determine the boundaries at which mangroves show a competitive growth advantage. Salinity is a major environment-limiting factor for mangrove growth because few plants except the mangrove can grow in high salinity environments (Lugo, 1998).

Second, Henderson (1966) indicated that the mechanism of mudflat formation involves secondary flows, which lead to mud accumulation on convex banks. When the flow in a curved channel, the presence of centrifugal force causes superelevated water surface. As a consequence, non-equilibrium between lateral pressure and centrifugal force results in secondary flow occurrence. The secondary flow would bring bed materials from concave bank to convex bank (Yen, 1965) and encourage an environment for creation and maintenance of physical habitat (Bockelmann et al., 2004). According to our observation in the Tanshui River system, mangrove areas were located on convex banks in meander bends. Therefore, the phenomenon of secondary flow may have a strong relationship with mangrove area formation. The index of *R*/*W* (ratio of radius of curvature to river width) was established as the second threshold. A strong relationship between *R*/*W* value and secondary flow has been found (Bagnold, 1960).

Finally, coverage ratios of mangrove on these screened mudflats from the previous analysis were calculated by using aerial photo interpretation and field survey calculation. Mangrove growth on mudflats may be controlled by other environmental conditions (e.g., slope, topography, flooding, prolonged hydroperiods, nutrient concentration, and the accumulation of toxic substances, such as H_2S) (Lugo, 1998; Lewis, 2005; Chen et al., 2006; Kamali and Hashim, in press) or may be changed to terrestrial plants due to secondary succession (Lewis, 2005). These mudflats show low coverage ratio and are classified as potential mangrove areas. On the contrary, mangroves flourished on mudflats that are slightly controlled by other environmental conditions and were thus classified as mangrove areas. Indeed, potential mangrove areas might become mangrove areas by removing the existing limiting factors through man-made restoration projects.

2.2.1. Salt intrusion simulation

Based on the NETSTARS model (Network of Stream Tube Model for Alluvial River Simulation) (Lee et al., 1997) and the suggestions of our previous research for parameter settings (Lee et al., 1998), the distribution of salinity in the Tanshui River system was simulated. The NETSTARS is a quasi-two-dimensional model and uses the de Saint Venant equation, the continuity equation and the momentum equation for unsteady flow calculation. It has been successfully applied to networking rivers in hydrodynamic, sediment transport and salinity simulations (Hong, 1998; Hsu et al., 1999; Lin et al., 2005; Shih et al., 2008; Hsu and Hsu, 2009).

For salinity intrusion simulation, there are two model parameters in the NETSTARS model, Manning's *n* values and the longitudinal dispersion coefficients, should be validated. There were two intensive field measurements in 1994 for water velocity, depth and salinity. The data of four measure-stations, such as river mouth, Guandu Bridge, Pailing Bridge and Hsinhai Bridge were included (Fig. 1). There were more than three measure-points in each measure-station. In addition, each measure-point had five sample-points vertically, including 0.1 h, 0.3 h, 0.5 h, 0.7 h and 0.9 h. The data was took every 30 min during a while tidal period. We used these two complete measurements to validate the model parameters.

The model adopted cross-section bathymetry of the Tanshui River system in 1994 as the topographic data. In order to simulate the distribution of mean annual salinity concentration for salinity intrusion, the downstream boundary condition was determined by the tidal level data over 8760 h in 1994 from a gauge station near the river mouth. The upstream boundary conditions were determined by annual mean discharge in 1994 from gauge stations near T050 for the Dahan Creek, near the NEW-S017A for Hsindian Creek, and near K079 for the Keelung River (data source: Northern Region Water Resources Office, Water Resources Agency, Taiwan). The annual mean discharges were 40.32 cm for the Dahan Creek, 70.52 cm for the Hsindian Creek, and 25.65 cm for the Keelung River, respectively.

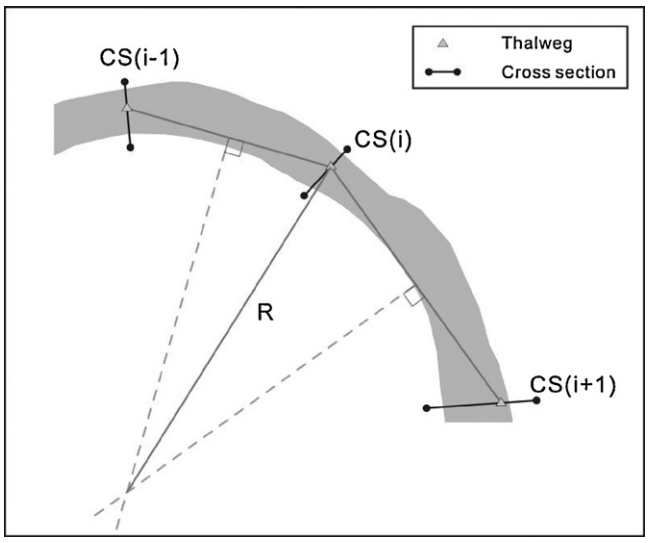

Fig. 3. Schematic plot of quantification for the radius of curvature. Find out the intersection of two perpendicular bisectors of the line of maximum depth between CS($i-1$) and CS(i) and between CS(i) and CS($i+1$). The length between the intersection point and the maximum depth of CS(i) is the radius of curvature of CS(i).

2.2.2. The R/W value calculation

The radius of curvature was examined from aerial photos with three steps. First, drawing a perpendicular bisector of the line of maximum depth between CS($i-1$) and CS(i), and that between CS(i) and CS($i+1$). Second, finding an intersection point of these two perpendicular bisectors. Finally, calculating the length between the maximum depth of CS(i) and the intersection point, R. The details are illustrated in Fig. 3. Furthermore, the river width was calculated form NETSTARS with bank-full flow discharge.

$$\frac{R}{W} = \frac{\text{radius of curvature}}{\text{river width}} \tag{1}$$

2.2.3. Field survey and identification of mangroves: absence or presence

The existence of mangroves was identified at both of the uppermost boundaries surveyed and by the coverage ratio at a specific mudflat. In high salinity environment, *K. obovata* have competitive growth advantage due to special salt-excluding mechanism. On the other hand, the propagule of *K. obovata* disperses by tidal force from December to April. Environmental salinity and mangrove propagule dispersal are controlled by tidal force. While salinity concentration and tidal force decreases as the distance from the river mouth increases, an uppermost boundary for mangrove expansion exists. In this study, the uppermost boundaries were determined by a field survey from July to August 2007. The criterion for successful growth of *K. obovata* was defined as the survival of more than one sapling with grown roots and leaves (Krauss et al., 2008).

The area of our field survey started from a known mangrove area and continued to the uppermost boundary of salinity intrusion calculated by the NETSTARS model along both the right and left banks. The uppermost boundary, the density of the mangroves and the height of canopies were recorded.

In addition, the coverage ratio of the mangroves (CR_{mg}) was used to determine their competitive growth advantage in that mudflat. This could be simplified as a ratio that represents a length of mangrove growth (L_{mg}) relative to a length of viable mudflat (L_{mf}), as shown in Eq. (2).

$$CR_{mg} = \frac{L_{mg}}{L_{mf}}; \quad 0 < L_{cr} \leq 1 \tag{2}$$

where L_{mf}, a mudflat length between the mean water level and the mean high water level (Lear and Turner, 1977), was calculated according to the cross-section bathymetry with the tidal level by the NETSTARS model simulation, as shown in Fig. 4(a). L_{mg}, a length of mangrove growth, was quantified from aerial photos and confirmed by the field survey, as shown in Fig. 4(b).

3. Results

3.1. Absence or presence of mangrove K. obovata

According to the field survey, the uppermost boundaries of *K. obovata* growth on the left and right banks along the Tanshui River were both around 19.5 km from the river mouth, and the left and right banks along the Keelung River were around 14.0 km and 14.5 km from the river mouth, respectively. No *K. obovata* was discovered along the Dahan and Hsindian Creek. The uppermost boundaries and situations of *K. obovata* growth are shown in Table 1. As the distance from the river mouth along the Tanshui River increased, the area of *K. obovata* growth declined, and the mangroves gradually started to grow with other vegetations, such as reeds. Along the Keelung River, there were no large areas of *K. obovata*, except for the Guandu wetland. Reeds mostly occupied the mudflats at some confluences of small tributaries, at some exits

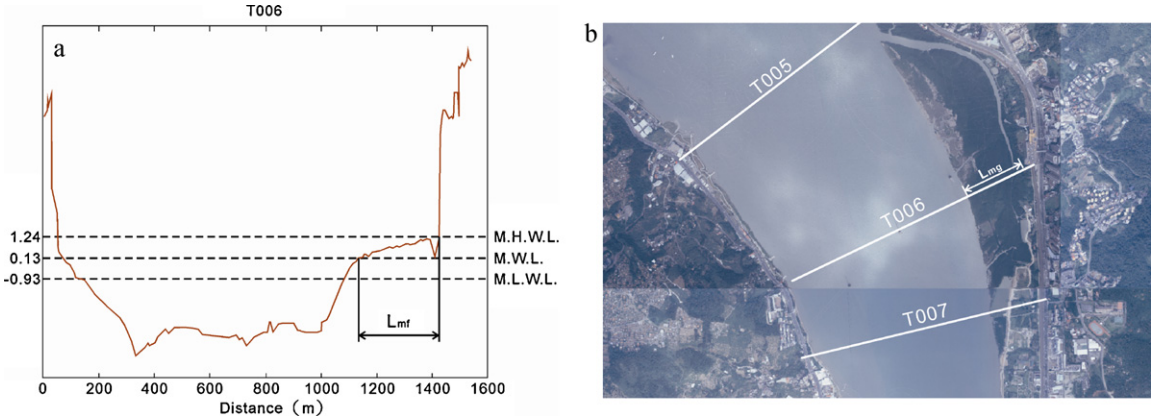

Fig. 4. Illustration of how the length of the viable mudflat (L_{mf}) and mudflat growth (L_{mg}) were determined. (a) Digitized L_{mf} between the mean water level and the mean high water level. Cross-section topography data were provided by the Water Resources Agency. The water level was obtained from the NETSTARS model simulation. M.H.W.L. is the mean high water level; M.W.L. is the mean water level, and M.L.W.L. is the mean low water level. (b) The L_{mg} of each cross-section was interpreted through aerial photographs and field measurements. Aerial photographs were obtained from the Aerial Survey Office of the Forestry Bureau.

Table 1
Uppermost boundaries and growth statuses of *K. obovata*. According to the field measurement between July and August 2007, the uppermost boundaries on the right and left banks of the Tanshui River were the same, but there was a slight difference between those on the right and left banks of the Keelung River. In general, the density of *K. obovata* showed a sparse distribution around the uppermost boundary.

River reach		Distance from the river mouth (km)	Height of canopy (m)	Density
Tanshui River	Right bank	19.5	1.4	Sparse distribution (<0.5 plant/m^2)
	Left bank	19.5	1.3	Sparse distribution (<0.5 plant/m^2)
Dahan Creek	Right bank	–	–	No mangroves
	Left bank	–	–	No mangroves
Hsindian Creek	Right bank	–	–	No mangroves
	Left bank	–	–	No mangroves
Keelung River	Right bank	14.5	0.7	≈1 plant/m^2
	Left bank	14.0	1.8	≈1 plant/m^2

of the water's gate, and at some accumulated sediments between gabion dikes, but some sparse *K. obovata* were still found with reeds.

3.2. Water salinity distribution

3.2.1. NETSTARS model validation

The model validation process involved tuning of Manning's *n* values and longitudinal dispersion coefficients and consisted of two parts: calibration and verification. The salinity data in June 24, 1994 for calibration was collected from the four measure-stations and the data in April 12, 1994 for verification was from three measure-stations. The validation results were compared with two intensive field measurements, as shown in Fig. 5. The results show that the NETSTARS model can successfully simulate the salinity distribution of the Tanshui River system because salinity concentrations obtained by the simulation matched those measured.

3.2.2. Salinity distribution and the mangrove coverage ratio

From NETSTARS' prediction, the terminal of salinity intrusion (salinity < 0.1 ppt) for the Dahan Creek, the Keelung River, and the Hsindian Creek were discovered as 21.5 km, 15.7 km, and 21.9 km from the river mouth, respectively (Fig. 6). The curve in Fig. 6 also presents the distribution of mean annual salinity concentration. The terminal of salt intrusion for the Tanshui River was very close to the confluence of the Dahan Creek and the Hsindian Creek. There was no salt water in the Dahan and Hsindian Creek. On the other hand, the salinity decreased very quickly along the Keelung River.

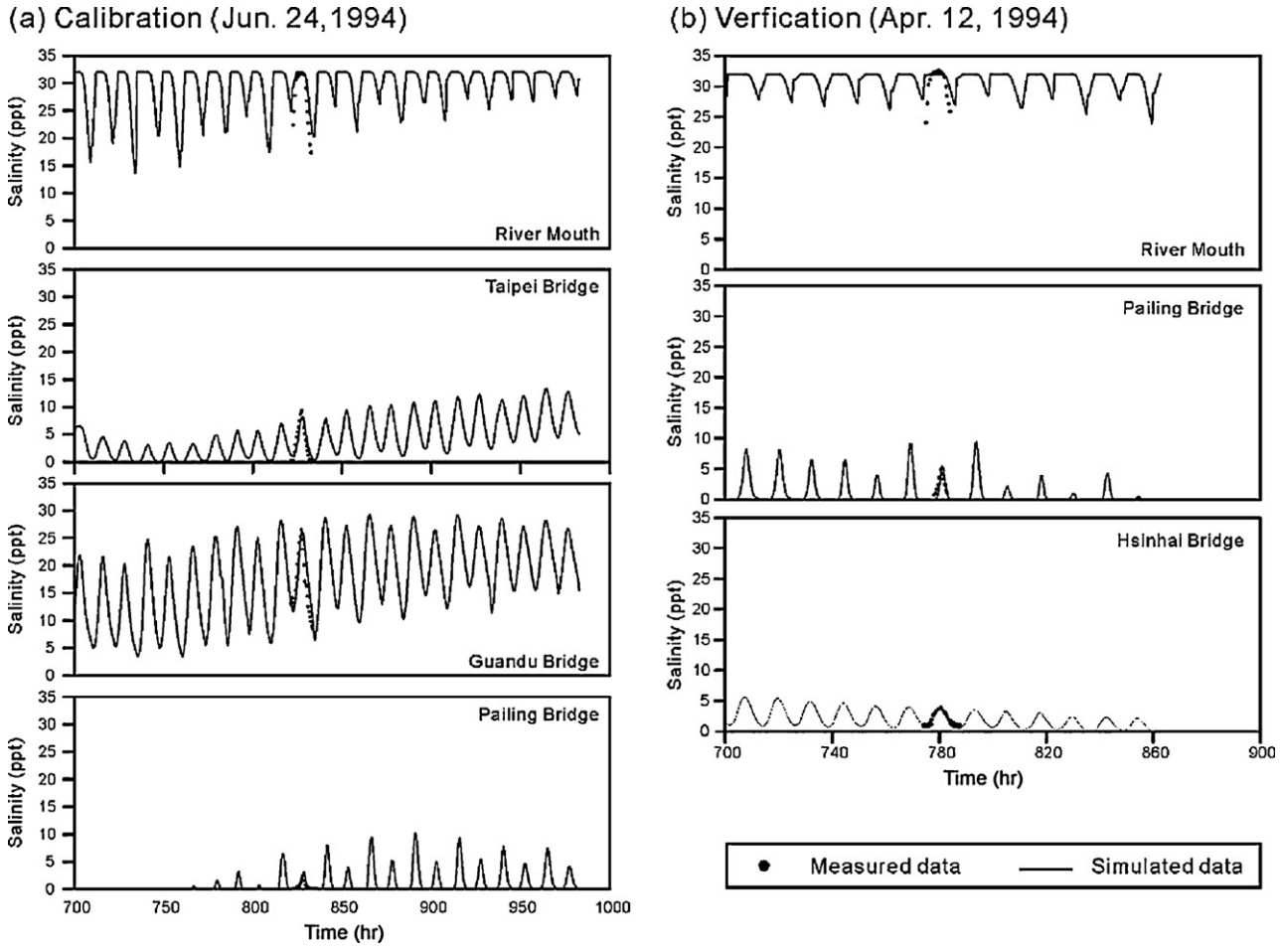

Fig. 5. The calibration and verification results of NETSTARS model simulation. The salinity concentration distributions from the intensive field measurements (June 24, 1994) were used for the calibration process, and the data for a different time (April 12, 1994) were examined for the verification process.

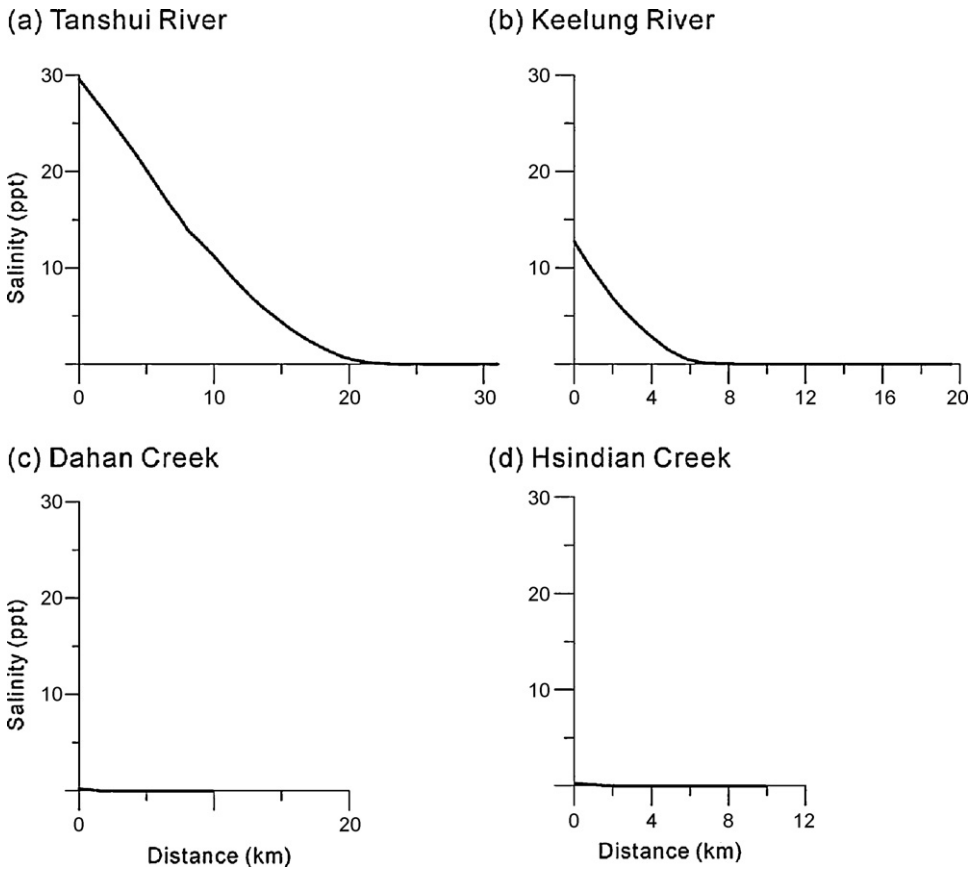

Fig. 6. NETSTARS predictions for salinity distribution of Tanshui River system. (a) The Tanshui River (including the Dahan Creek); (b) the Keelung River; (c) the Dahan Creek; (d) and the Hsindian Creek. The distance of the *x*-axis for the Tanshui River is calculated from the river mouth. The distance for the Keelung River, the Dahan Creek and the Hsindian Creek is calculated from the confluence. The terminals were located 21.5 and 15.7 km from the river mouth for the Tanshui and Keelung Rivers, respectively. Furthermore, there was almost no salt water found in the Dahan Creek or the Hsindian Creek.

The distance of the intrusion was around 6.6 km from the confluence of the Keelung River.

On the other hand, there were no large (though spotted) areas of *K. obovata* growth beyond a specific distance from the river mouth (Fig. 7). The uppermost boundary for *K. obovata* with a competitive growth advantage (UBC) is where the mean annual salinity level is 5 ppt. The uppermost boundary for *K. obovata* growth (UB) is where the mean annual salinity level is 0.1 ppt. The bar chart in Fig. 7 shows the coverage ratio of *K. obovata* and the relevant distance from river mouth for the Tanshui and Keelung Rivers, respectively. Though the tendency of the coverage ratio cannot be clarified obviously from the figures, it is clear that large areas of *K. obovata* habitat does not appear beyond a specific distance from the river mouth, i.e., UBC.

3.3. Secondary flow intensity – R/W values

Analysis area was limited to river reaches where mangroves have growth competitive advantage. In the other words, mean annual salinity of these reaches were higher than 5 ppt. The reach lengths were approximately 14.5 km and 11.1 km from the river mouth along the Tanshui River and the Keelung River, respectively (Fig. 8).

Table 2 shows the calculated result of *R*/*W* within the area of interesting. The measurements of river width were taken from the simulation results of bank-full flow discharge with a 2-year return period flood. The radius of curvature varied from 767 m at T007 to 375,126 m at T009. In Tanshui River, lower *R*/*W* values from T003 to T008 indicated that the Tanshui River turns left around Zhuwei, and from T013 to T014 represented that the Tanshui River turns right before the confluence of the Keelung River. In addition, in the Keelung River, lower *R*/*W* values from K001 to K002 illustrated that the Keelung River turns right before the confluence of the Tanshui River.

4. Discussion

4.1. The relationship between salinity and spreading capability

K. obovata had a competitive growth advantage along the Tanshui River system, with mean annual salinity that was higher than 5 ppt according to a comparison between the water salinity from simulation and the coverage ratio from our calculations. Indeed, *K. obovata* showed a competitive growth advantage within approximately 14.5 km and 11.1 km from the river mouth along the Tanshui River and the Keelung River, respectively. This suggests that a mean annual salinity higher than 5 ppt is one of the thresholds for the spreading capability of *K. obovata*, a finding which was supportive to other research (Qiu et al., 2005; Ru et al., 2009).

Moreover, the uppermost boundary of *K. obovata* growth was also controlled by the mean annual salinity. According to the field survey, the uppermost boundaries were approximately 19.5 km and 14.5 km from the river mouth along the Tanshui River and the Keelung River, respectively. On the other hand, the terminals of salinity intrusion were approximately 21.5 km and 15.7 km from the river mouth along the Tanshui River and the Keelung River,

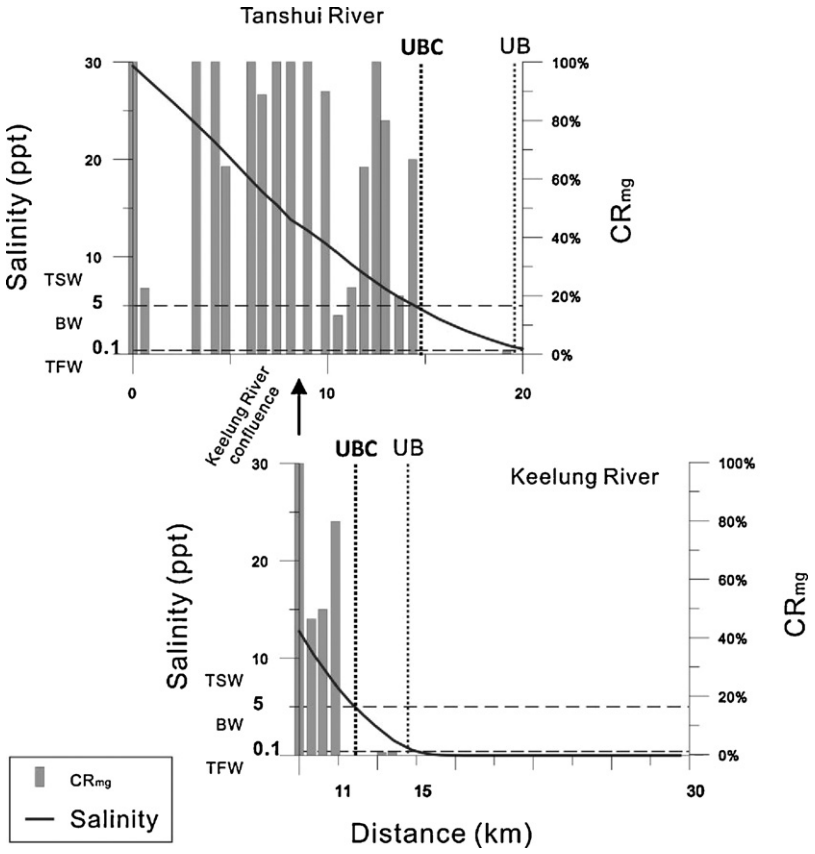

Fig. 7. Relationship between salinity distribution and the coverage ratio of *K. obovata*. The distance of the *x*-axis for the Tanshui River is calculated from the river mouth. The arrow shows the confluence between the Tanshui River and the Keelung River. The left *y*-axis shows the water salinity concentration, and the right *y*-axis shows the coverage ratio. The uppermost boundary for *K. obovata* with a competitive growth advantage (UBC) is where the mean annual salinity level is 5 ppt. The uppermost boundary for *K. obovata* growth (UB) is where the mean annual salinity level is 0.1 ppt. TSW, BW, TFW are the tidal saltwater wetland, the brackish wetland, and the tidal freshwater wetland, respectively.

Table 2
Calculated results of the *R*/*W* value in different cross-sections. The radius of curvature was quantified from the aerial photo and river width was measured form simulated results with bank-full flow discharge. The *R*/*W* value lower than 3 is indicated in bold and presents that inner bank separation and secondary flow may occur.

River reach	Sites	Distance from the river mouth (km)	Radius of curvature, *R* (m)	River width, *W* (m)	*R*/*W*
	T001	0.62	24,435	1498	>10.00
	T002	1.21	5222	1448	3.61
	T003	**1.86**	**2826**	**1228**	**2.30**
	T004	**2.57**	**2617**	**1317**	**1.99**
	T005	**3.25**	**1253**	**1087**	**1.15**
	T006	**4.23**	**1402**	**1370**	**1.02**
	T007	**4.77**	**767**	**1094**	**0.70**
	T008	**5.29**	**2045**	**821**	**2.49**
	T009	6.08	375,126	558	>10.00
	T010	6.63	3541	608	5.83
Tanshui River	T011	7.38	6613	523	>10.00
	T012	8.10	4684	427	>10.00
	T013	**8.97**	**1177**	**1031**	**1.14**
	T014	**9.88**	**1038**	**969**	**1.07**
	T015	10.52	3789	843	4.49
	T016	11.22	4187	791	5.30
	T017	11.86	3617	688	5.26
	T018	12.49	7130	502	>10.00
	T019	12.95	6885	364	>10.00
	T020	13.65	3441	530	6.49
	T021	14.35	3107	602	5.16
	K001	**9.10**	**1534**	**603**	**2.54**
Keelung River	**K002**	**9.85**	**1294**	**439**	**2.95**
	K003	10.71	2187	258	8.48

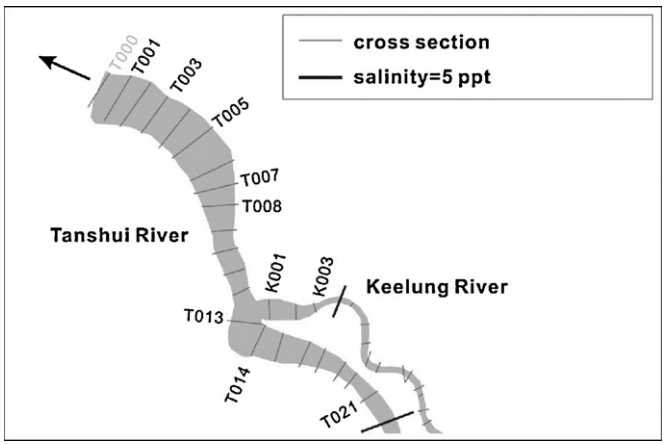

Fig. 8. Location of cross-sections along the Tanshui River and the Keelung River. The analysis area of secondary flow occurrence was limited within the reach where mean annual salinity are higher than 5 ppt, i.e. the uppermost boundary for *K. obovata* with a competitive growth advantage (UBC).

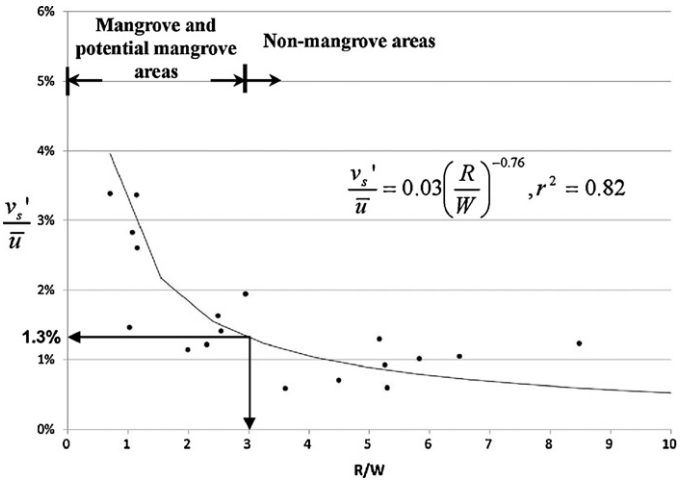

Fig. 9. Relationship between the R/W values and the dimensionless velocity of secondary flow along the Tanshui River system. When the R/W value is lower than 3, the velocity the secondary flow would increase rapidly. The areas which R/W lowers than 3 are distinguished as "mangrove or potential mangrove areas" which others are "non-mangrove areas". The critical $v_s'/\bar{u}$ is 1.3% which implies that the mudflat generates when the velocity of secondary flow occupies more than 1.3% of longitudinal flow.

respectively. This shows that the uppermost boundaries were close to the terminal of salinity intrusion. Furthermore, no *K. obovata* was discovered in the Dahan Creek and the Hsindian Creek, as these are located higher than the terminal of salinity intrusion. Our results show that although propagules of *K. obovata* can germinate with no salinity conditions in the lab (Wang et al., 2004), *K. obovata* cannot survive without water salinity conditions in nature, corresponding to the results of a field survey in Fujian, China (Lin and Wei, 1981).

We concluded that the riparian wetlands of the Tanshui River system can be divided into three categories according to the spreading capability of *K. obovata*: (1) tidal saltwater wetlands with mean annual salinity levels higher than 5 ppt are riparian wetlands in which *K. obovata* cannot only grow but also has a competitive growth advantage; (2) brackish wetlands with mean annual salinity levels of between 5 and 0.1 ppt are riparian wetlands in which *K. obovata* can survive; (3) tidal freshwater wetlands with mean annual salinity levels that are lower than 0.1 ppt are riparian wetlands in which *K. obovata* cannot survive naturally.

4.2. The relationship between the R/W values and mangrove areas identification

We found that large mudflats will be formed when the R/W value is lower than 3. The R/W value of major mangrove areas, i.e. T003–T008, T013–T014 and K001–K002, was lower than 3 (Table 3). The results proved that mudflat formation was controlled by secondary flow and bare mudflats might facilitate *K. obovata* invasion.

Furthermore, the mangrove ratios of T007 and K002 reveal only 64% and 47% occupation and imply that these two areas might have high spreading capability. They would become pure mangrove forests in the future as current situations of T005, T006, T013 and K001 or change to terrain plants due to secondary succession as (Lewis, 2005) mentioned. We also discovered that mangroves did not appear in the sites of T003, T004 and T008 due to human disturbance such as the riverside park or farm land constructions. These areas were classified to be potential mangrove areas.

4.3. The R/W values compare with velocity of secondary flow

The equations developed by Odgaard (1986a,b) were employed to measure the velocity of secondary flow with steady, subcritical, and turbulent condition in a meandering alluvial channel and employed to examine the physical meaning of R/W as shown in Eqs. (3) and (4).

$$v_s' = \frac{\alpha}{2}\bar{u} \tag{3}$$

$$\alpha = \frac{2m+1}{\kappa^2 m}\cdot\frac{d}{R} \tag{4}$$

where v_s', centrically induced velocity of water surface corresponding to no net transverse mass transport. $\bar{u}$ and d, depth-averaged mean velocity along the channel centerline and water depth, were taken from the results of model simulation. m, velocity-profile exponent within the range 3–7 ($m = \kappa \cdot C/\sqrt{g}$), k, von Karman's constant, equals to 0.4 with homogeneous fluid. The value, m, was set 5 as $k = 0.4$ and $C = 40$ (C, Chezy's coefficient, is equal to around 40 in the study area).

We derived a dimensionless regression equation between R/W and $v_s'/\bar{u}$ as shown in Eq. (5). A high negative correlation ($r^2 = 0.82$) and power law relationship was found. While the negative correlation points out that the R/W values and velocity of secondary flow have adverse tendency. High velocity of secondary flow often leads to the formation of mudflats, which might facilitate mangrove invasion through the creation of bare mudflats. We also found that the mudflat generated when the dimensionless velocity of secondary flow increases to 1.3% (Fig. 9).

$$\frac{v_s'}{\bar{u}} = 0.03\left(\frac{R}{W}\right)^{-0.76}, \quad r^2 = 0.82 \tag{5}$$

4.4. The sea level rise effect and its impact

Because rising sea level enhances salt intrusion, the capability of mangrove invasion is expected to increase and may cause the vegetation to shift toward mangrove. For example, at the central part of the Braganca peninsula in Brazil, a large area (approximately 3.2 km^2 and 36% of the original area) had been occupied by the mangrove *Avicennia germinans* from 1972 to 1992 (Lara et al., 2002). In the Tanshui River system, a wetland located in the confluence of the Tanshui River and the Hsindian Creek might be occupied by the *K. obovata*. In addition, *K. obovata* may appear within riparian wetlands of the Dahan Creek and the Hsindian Creek. The original riparian vegetation will face more serious threats by mangrove

Table 3
Possible locations of mangrove area and identification of mangrove areas for the Tanshui River system. The CR_{mg} value is a ratio that presents a length of mangrove growth (L_{mg}) relative to a length of viable mudflat (L_{mf}) to determine their competitive growth advantage in that mudflat. The SSA model selects three mangrove areas (Zhuwei wetland, T005–T008; Shezi wetland, T013–T014; Guandu wetland, K001–K002) and two potential mangrove areas located in the Tanshui River (T003–T004 and T008). They are consistent with the current situation.

River reach	Sites	Distance from the river mouth (km)	R/W	L_{mf} (m)	L_{mg} (m)	CR_{mg}	Mangrove areas identification
Tanshui River	T003	1.86	2.30	0	0	0%	Potential mangrove area
	T004	2.57	1.99	0	0	0%	
	T005	3.25	1.15	210	210	100%	Mangrove area (Zhuwei wetland)
	T006	4.23	1.02	275	275	100%	
	T007	4.77	0.70	140	90	64%	
	T008	5.29	2.49	70	0	0%	Potential mangrove area
	T013	8.97	1.14	30	30	100%	Mangrove area (Shezi wetland)
	T014	9.88	1.07	100	90	90%	
Keelung River	K001	9.10	2.54	400	400	100%	Mangrove area (Guandu wetland)
	K002	9.85	2.95	150	70	47%	

invasion. In contrast, mangroves may die in lower elevation mudflats because the original mudflats may be over-inundated by the rising sea level (Bird, 1993; Ellison, 1993).

Although knowledge of species distributions in climate change is very important (Austin, 2007), it is difficult to predict the future of mangrove forests due to the lack of long-term data available (Alongi, 2002). The sea level rise effect might be a vital environment factor for mangrove wetland management.

5. Summaries

A new salinity-secondary flow-approach (SSA) model was developed to identify mangrove areas, potential mangrove areas, and non-mangrove areas by two indices: mean annual salinity and R/W value. We applied the SSA model in the Tanshui River system and found that riparian wetlands with salinity values greater than 5 ppt and R/W values lower than 3 are best suited for the survival and spreading of *K. obovata*. These selected mangrove areas are now the main mangrove forests of *K. obovata*: the Zhuwei wetland (T005–T007) and the Shezi wetland (T013–T014) in the Tanshui River and the Guandu wetland (K001–K002) in the Keelung River. Furthermore, some potential mangrove areas were also found (T003, T004, and T008). Mangroves did not appear there due to human disturbance such as the riverside park or farm land constructions.

Mangroves might extend rapidly and exclude other species in the selected mangrove areas, because they have competitive growth advantage. Management policy is suggested to avoid ecological and flooding impacts. On the other hand, a potential mangrove area might be a good location for restoration project, because this area is suitable for mangrove growth form saline and morphological point of view. A planting phase in a successful restoration project may not necessary when the stressors are removed and suitable hydrological conditions are provided (Mitsch et al., 2005). Therefore, increasing successful probability and cost-effective for a restoration project can be achieved.While the SSA model is applied to other places, the two thresholds of mean annual salinity and R/W value might be slightly changed due to different mangrove species and characteristic of river morphology. Indeed, the dividing results of the same river system might be shifted in the future due to sea level rise. Some salt-sensitive vegetations of freshwater wetlands might exhibit stress or mortality due to saltwater intrusion (McKee and Mendelssohn, 1989; Baldwin and Mendelssohn, 1998). With mudflat formation, it is possible that *K. obovata* would spread further up the stream.

Acknowledgements

This research was funded by the National Science Council, Taiwan (NSC 98-2627-B-002-008 and NSC 99-2627-B-002-001), and the Water Resources Planning Institute, WRA, MOEA (MOEA/WRA-0960233). We deeply appreciate the support from these grants. We also thank the Tenth River Management Office of WRA, MOEA for providing the data of cross-sectional bathymetry, flow discharge records and water level records. The useful suggestions from two anonymous reviews have been incorporated into the manuscript.

References

Alongi, D.M., 2002. Present state and future of the world's mangrove forests. Environ. Conserv. 29, 331–349.
Austin, M., 2007. Species distribution models and ecological theory: a critical assessment and some possible new approaches. Ecol. Modell. 200, 1–19.
Bagnold, R.A., 1960. Some Aspects of the Shape of River Meanders. U.S. Govt. Print. Off., Washington.
Baldwin, A.H., Mendelssohn, I.A., 1998. Effects of salinity and water level on coastal marshes: an experimental test of disturbance as a catalyst for vegetation change. Aquat. Bot. 61, 255–268.
Bird, E.C.F., 1993. Submerging Coasts: The Effects of a Rising Sea Level on Coastal Environments. John Wiley & Sons, Chichester, New York.
Blasco, F., Saenger, P., Janodet, E., 1996. Mangroves as indicators of coastal change. CATENA 27, 167–178.
Bockelmann, B.N., Fenrich, E.K., Lin, B., Falconer, R.A., 2004. Development of an ecohydraulics model for stream and river restoration. Ecol. Eng. 22, 227–235.
Brown, S., Lugo, A.E., 1994. Rehabilitation of tropical lands: a key to sustaining development. Restor. Ecol. 2, 75–136.
Chen, L., Yang, Z., Wang, W., Lin, P., 2006. Critical tidal level for planting *Kandelia candel* seedlings in Xiamen. Chin. J. Appl. Ecol. 17, 177–181 (in Chinese with English abstract).
Clarke, L.D., Hannon, N.J., 1967. Mangrove swamp and salt marsh communities of Sydney district. I. Vegetation soils and climate. J. Ecol. 55, 753–771.
Duke, N.C., Lo, E.Y.Y., Sun, M., 2002. Global distribution and genetic discontinuities of mangroves—emerging patterns in the evolution of Rhizophora. Trees-Struct. Funct. 16, 65–79.
Ellison, J.C., 1993. Mangrove retreat with rising sea-level Bermuda. Estuar. Coast. Shelf Sci. 37, 75–87.
Fan, K.C., 2006. An application of mangrove rehabilitation for Taiwan. Taiwan For. J. 32, 4–11 (in Chinese).
Guisan, A., Zimmermann, N.E., 2000. Predictive habitat distribution models in ecology. Ecol. Modell. 135, 147–186.
Henderson, F.M., 1966. Open Channel Flow. Macmillan, New York.
Hong, J.C., 1998. Dynamic Simulation of Water Quality in Tidal Reach of Tanshui River. Civil Engineering. Nation Taiwan University, Taipei, Taiwan (in Chinese).
Hsu, M.H., Kuo, A.Y., Kuo, J.T., Liu, W.C., 1999. Procedure to calibrate and verify numerical models of estuarine hydrodynamics. J. Hydraul. Eng.-Asce 125, 166–182.
Hsu, W.B., 2002. The Guide Book of the Nature Environment at Guandu: The Culture and Ecology. The Yu-shan Society publication Inc (in Chinese).
Hsu, Y.S., Hsu, Y.H., 2009. Impact of earthquake-induced dammed lakes on channel evolution and bed mobility: case study of the Tsaoling landslide dammed lake. J. Hydrol. 374, 43–55.

Hsueh, M.L., Lee, H.H., 2000. Diversity and distribution of the mangrove forests in Taiwan. Wetlands Ecol. Manage. 8, 233–242.
Huang, S.C., Shih, S.S., Ho, Y.S., Chen, C.P., Hsieh, H.L., 2010. Restoration of shorebird-roosting mudflats by partial removal of estuarine mangroves in Northern Taiwan. Restor. Ecol., doi:10.1111/j.1516-100X.2010.00744.X.
Hupp, C.R., Osterkamp, W.R., 1996. Riparian vegetation and fluvial geomorphic processes. Geomorphology 14, 277–295.
Kamali, B., Hashim, R., in press. Mangrove restoration without planting. Ecol. Eng.
Krauss, K.W., Lovelock, C.E., McKee, K.L., Lopez-Hoffman, L., Ewe, S.M.L., Sousa, W.P., 2008. Environmental drivers in mangrove establishment and early development: a review. Aquat. Bot. 89, 105–127.
Lara, R., Szlafsztein, C., Cohen, M., Berger, U., Glaser, M., 2002. Implications of mangrove dynamics for private land use in Braganca, North Brazil: a case study. J. Coast. Conservat. 8, 97–102.
Lear, R.J.C., Turner, T., 1977. Mangroves of Australia. University of Queensland Press, St. Lucia Australia.
Lee, C.T., Cheng, Y.P., Chiou, W.L., Lin, T.T., 2002. Vegetation changes at the Kuantu nature reserve during 1986–1998. Taiwan For. J. 17, 41–50 (in Chinese).
Lee, C.T., Chu, T.H., 1999. A Study of Changes of the Mangorve Distribution *Kandelia candel* (L.) Druce in Tanshui Estuary—A Geomorphologic Perspective. National Science Council (in Chinese with English abstract).
Lee, H.Y., Hsieh, H.M., Yang, J.C., Yang, C.T., 1997. Quasi-two-dimensional simulation of scour and deposition in alluvial channels. J. Hydraul. Eng.-Asce 123, 600–609.
Lee, H.Y., Lee, S.Y., Hsieh, H.M., 1998. Numerical Simulation of the Hydraulic Characteristics of a Estuarine River Network. Hydroinformatics98, Denmark.
Lee, H.Y., Shih, S.S., 2004. Impacts of vegetation changes on the hydraulic and sediment transport characteristics in Guandu mangrove wetland. Ecol. Eng. 23, 85–94.
Lee, T.M., Yeh, H.C., 2009. Applying remote sensing techniques to monitor shifting wetland vegetation: a case study of Danshui River estuary mangrove communities, Taiwan. Ecol. Eng. 35, 487–496.
Lewis, R.R., 2000. Ecologically based goal setting in mangrove forest and tidal marsh restoration. Ecol. Eng. 15, 191–198.
Lewis, R.R., 2005. Ecological engineering for successful management and restoration of mangrove forests. Ecol. Eng. 24, 403–418.
Lin, P., Wei, S.M., 1981. A reseach about subtropical biology of mangrove in Fujian, China. Plant Ecol. Geobotany 5, 177–186 (in Chinese).
Lin, Y.J., Lai, J.S., Lee, H.Y., Ho, H.C., Lee, F.T., 2005. An Experimental Study on the Movement of Turbidity Current. AOGS2005, Singapore.
Liu, W.C., Chen, W.B., Cheng, R.T., Hsu, M.H., Kuo, A.Y., 2007. Modeling the influence of river discharge on salt intrusion and residual circulation in Danshuei River estuary, Taiwan. Cont. Shelf Res. 27, 900–921.
Lugo, A.E., 1998. Mangrove forests: a tough system to invade but an easy one to rehabilitate. Mar. Pollut. Bull. 37, 427–430.
McKee, K.L., Mendelssohn, I.A., 1989. Response of a fresh-water marsh plant community to increased salinity and increased water level. Aquat. Bot. 34, 301–316.
Mitsch, W.J., 2005. Applying science to conservation and restoration of the world's wetlands. Water Sci. Technol. 51, 13–26.
Mitsch, W.J., Day, J.W., 2006. Restoration of wetlands in the Mississippi-Ohio-Missouri (MOM) river basin: experience and needed research. Ecol. Eng. 26, 55–69.
Mitsch, W.J., Gosselink, J.G., 1993. Wetlands. Van Nostrand Reinhold Co.
Mitsch, W.J., Zhang, L., Anderson, C.J., Altor, A.E., Hernandez, M.E., 2005. Creating riverine wetlands: ecological succession, nutrient retention, and pulsing effects. Ecol. Eng. 25, 510–527.
Odgaard, A.J., 1986a. Meander flow model. 1. Development. J. Hydraul. Eng.-Asce 112, 1117–1136.
Odgaard, A.J., 1986b. Meander flow model. 2. Applications. J. Hydraul. Eng.-Asce 112, 1137–1150.
Perdomo, L., Ensminger, I., Espinosa, L.F., Elster, C., Wallner-Kersanach, M., Schnetter, M.L., 1998. The mangrove ecosystem of the Cienaga Grande de Santa Marta (Colombia): observations on regeneration and trace metals in sediment. Mar. Pollut. Bull. 37, 393–403.
Qiu, D.L., Lin, P., Su, J.W., 2005. Relationship of leaf ultrastructure of mangrove *Kandelia candel* (L.) Druce to salt tolerance. J. For. Sci. 51, 476–480.
Ren, H., Lu, H.F., Shen, W.J., Huang, C., Guo, Q.F., Li, Z.A., Jian, S.G., 2009. *Sonneratia apetala Buch.Ham* in the mangrove ecosystems of China: an invasive species or restoration species. Ecol. Eng. 35, 1243–1248.
Ru, Q.M., Xiao, Q., Lin, P., Pei, Z.M., Zheng, H.L., 2009. Short- and long-term effects of NaCl on physiological and biochemical characteristics in leaves of a true mangrove, *Kandelia candel*. Russ. J. Plant. Physl. 56, 363–369.
Sheue, C.R., Liu, H.Y., Yong, J.W.H., 2003. *Kandelia obovata* (*Rhizophoraceae*), a new mangrove species from Eastern Asia. Taxon 52, 287–294.
Shih, S.S., Lee, H.Y., Chen, C.C., 2008. Model-based evaluations of spur dikes for fish habitat improvement: a case study of endemic species *Varicorhinus barbatulus* (*Cyprinidae*) and *Hemimyzon formosanum* (*Homalopteridae*) in Lanyang River, Taiwan. Ecol. Eng. 34, 127–136.
Shih, S.S., Yu, W.S., 2008. Spatial Distribution and Reuse Assessment of Riverbed Sludge of Tanshui River System. Water Resource Agency, Taipei, Taiwan (in Chinese).
Wang, L.Y., Chen, J.L., Lee, M.J., 2004. Effects of salinity on growth of seedlings of *Kandelia Candel* (L.) Druce. Taiwan For. J. 32, 147–155 (in Chinese).
Wester, L., Lee, C.T., 1992. Mangroves in Taiwan: distribution management and values. Geoforum 23, 507–519.
Yen, B.C., 1965. Characteristic of Subcritical Flow in a Meandering Channel. Institute of Hydraulic Research/University of Iowa, Iowa City.